PHYSICS

Optics-less focusing of XUV high-order harmonics

L. Quintard[1], V. Strelkov[2,3], J. Vabek[1], O. Hort[1]*, A. Dubrouil[1†], D. Descamps[1], F. Burgy[1], C. Péjot[1], E. Mével[1], F. Catoire[1‡], E. Constant[1,4‡]

By experimentally studying high-order harmonic beams generated in gases, we show how the spatial characteristics of these ultrashort extreme-ultraviolet (XUV) beams can be finely controlled when a single fundamental beam generates harmonics in a thin gas medium. We demonstrate that these XUV beams can be emitted as converging beams and thereby get focused after generation. We study this optics-less focusing using a spatially chirped beam that acts as a probe located inside the harmonic generation medium. We analyze the XUV beam evolution with an analytical model and obtain very good agreement with experimental measurements. The XUV foci sizes and positions vary strongly with the harmonic order, and the XUV waist can be located at arbitrarily large distances from the generating medium. We discuss how intense XUV fields can be obtained with optics-less focusing and how the order-dependent XUV beam characteristics are compatible with broadband XUV irradiation and attosecond science.

INTRODUCTION

It is now possible to generate extreme-ultraviolet (XUV) attosecond pulses via high-order harmonic generation (HHG) in gases with high photon flux (*1*–*3*). These XUV beams exhibit good spatial coherence, but their spatial properties (*4*–*11*) appear now as more complex than previously considered. Dedicated experiments and simulations are developed to understand and control the harmonic beam spatial properties (*8*–*14*). Harmonic-dependent wavefront curvature has recently been observed (*7*, *9*) experimentally, and direct XUV beam focusing has also been predicted via simulations with XUV-seeded harmonic generation (*13*) in gas. Performing optics-less XUV focusing using a single fundamental beam (*14*) to selectively focus some harmonics and thereby perform spectral filtering of attosecond pulses has also been proposed, but these predictions were not confirmed experimentally. Moreover, applications involving nonlinear processes (*15*–*18*) induced by high-order harmonics require high XUV intensities and good focusability of the XUV beams, which remain difficult to achieve. Improving the understanding and control of the spatial properties of the high-order harmonic beams is essential, and we show here experimentally that this control can provide optics-less focusing of XUV beams.

We study the impact of the macroscopic conditions of HHG in gases on the XUV beam's wavefront and spatial profiles. Experimentally, HHG is performed with a wavefront-corrected fundamental beam, and we observe a strong evolution of the XUV beam properties with harmonic order and generating conditions. A Gaussian model developed to infer the beam properties shows that both the divergence and beam waist position can be controlled. We demonstrate how and why the longitudinal position of the HHG gas medium dramatically affects the XUV beam.

In contrast to usual statements where high-order harmonic beams are considered as divergent after the generating medium, we show that harmonic beams, generated with a single fundamental beam, can converge after the generating medium and are then focused without any XUV optics. This XUV optics-less focusing is further studied by performing HHG with a spatially chirped fundamental beam that acts as a probe localized directly inside the generation medium. These results experimentally demonstrate that converging or diverging XUV beams can be obtained by XUV wavefront control.

RESULTS

Characterization of the far-field XUV beam size evolution

To perform HHG, we used a 40-fs full width at half maximum (FWHM) fundamental pulse centered at 800 nm with energy of 2 to 5 mJ loosely focused with a 2-m focal length spherical mirror. It results in a waist of W_0 = 83 μm with Rayleigh length Z_{r_ir} = 2.7 cm and a peak intensity of 5.6×10^{14} W/cm^2 at focus for a pulse energy of 2.5 mJ. The beam is focused onto a pulsed neon jet (nozzle diameter, 250 μm) mobile in the longitudinal direction over z_{jet} = ±75 mm [z_{jet} being the position of the jet with respect to the infrared (IR) focus position]. The IR beam is spatially filtered to achieve a Gaussian-like spatial profile, and a deformable mirror (ISP System) provides a λ/100 wavefront correction of the IR beam ensuring good wavefront control of the emitted XUV light. We analyze the spatial profile of each harmonic in the far field with a flat field spectrometer (see details in Materials and Methods).

Our experimental observations confirmed that the harmonic beam size in the far field evolves strongly with the longitudinal jet position (*4*). Harmonics arising from the short quantum path (*19*) emission were predominant for all z positions. Those emitted via the long quantum path were very divergent (*20*) and are not considered in this paper.

The beam size (Fig. 1) of plateau harmonics evolves regularly with the jet position and harmonic order. It exhibits a shallow minimum between z_{jet} = −30 mm (H29) and −40 mm (H35), followed by a maximum around z_{jet} = 20 to 25 mm and a decrease afterward. We observed that the positions of the maxima and minima change with harmonic order. The maximum beam size (8 to 13 mm) increases with the harmonic order up to the order 37 and decreases afterward (see the Supplementary Materials). The minimum beam size does not change substantially with the harmonic order, but the positions of the minima change.

The measurements also showed that the XUV photon flux was preserved between the beam size minima and maxima (see the Supplementary Materials). The far-field XUV beam shape can therefore be controlled without compromising the XUV flux.

[1]Université de Bordeaux, CNRS, CEA, Centre Laser Intenses et Applications (CELIA), 43 rue P. Noailles, 33400 Talence, France. [2]Prokhorov General Physics Institute of the Russian Academy of Sciences, 38, Vavilova Street, Moscow 119991, Russia. [3]Moscow Institute of Physics and Technology (State University), 141700 Dolgoprudny, Moscow Region, Russia. [4]Université de Lyon, Université Claude Bernard Lyon 1, CNRS, Institut Lumière Matière (ILM), 69622 Villeurbanne, France.
*Present address: ELI Beamlines Project, Institute of Physics, Czech Academy of Sciences, Na Slovance 1999/2, 182 21 Praha 8, Czech Republic.
†Present address : Femto Easy, Femto Easy SAS, Batiment Sonora, parc scientifique et technologique Laseris 1, 33114 Le Barp, France.
‡Corresponding author. Email: eric.constant@univ-lyon1.fr (E.C.); fabrice.catoire@u-bordeaux.fr (F.C.)

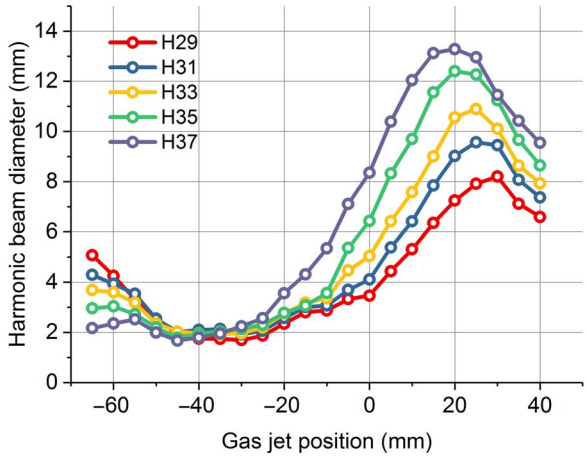

Fig. 1. Far-field XUV beam size. Measurement of the XUV beam size (FWHM) in the far field (i.e., 2.9 m after the IR focus) as a function of the longitudinal gas jet position with respect to the IR focus position. Harmonics are generated in a neon jet with a maximum intensity at focus of 5.6×10^{14} W/cm^2, and IR laser beam Rayleigh length of 2.7 cm.

Despite the simplicity of this experiment, the physics underlying the beam evolution is poorly understood, and phase matching, ionization, or beam reshaping is often invoked to explain this evolution. To capture this physics and predict the harmonic beam characteristics, we developed a model including collective effects but neglecting longitudinal phase matching and beam reshaping.

Simulations of the harmonic beam properties in the generating medium

The model that we developed is known to provide good qualitative results for HHG in a thin gas medium (*14*, *20*–*24*). The model dipole, d_q, of the harmonic with order q is given by

$$d_q(r,z) = I_{\mathrm{ir}}^{q_{\mathrm{eff}}/2}(z,r)\, e^{i(q\varphi_{\mathrm{ir}}(z,r) - \alpha_q I_{\mathrm{ir}}(z,r))} \quad (1)$$

where $I_{\mathrm{ir}}(z,r)$ is the intensity of the Gaussian fundamental beam at radial position r in the generation medium located at position z (z = 0 being the position of the focus of the IR beam), and q_{eff} is an effective order of nonlinearity. The phase, φ_q, of the harmonic dipole is q times the phase of the fundamental beam, φ_{ir}, plus the atomic contribution approximated by $\varphi_{\mathrm{atom}} = -\alpha_q I_{\mathrm{ir}}(z, r)$ (*19*, *20*).

This dipole provides the XUV field generated by an atom. The macroscopic response is obtained by considering an infinitely thin medium and by summing the contributions of many atoms located in the generation plane at various radial positions. In this approach, we neglect propagation in the medium as justified with a thin medium and loosely focused laser (see Materials and Methods). When the fundamental beam is Gaussian in the emission plane, with size $W_{\mathrm{ir}}(z)$, Eq. 1 ensures that the spatial profile of the XUV beam is also Gaussian in this plane with size

$$W_{\mathrm{XUV}}(z) = \frac{W_{\mathrm{ir}}(z)}{\sqrt{q_{\mathrm{eff}}}} \quad (2)$$

The spatial phase of a Gaussian fundamental beam has a quadratic evolution with r and a radius of curvature noted $R_{\mathrm{ir}}(z)$. Assuming that the harmonic emission takes place near the IR beam axis, the Gaussian intensity profile can be approximated by a parabolic profile (see Materials and Methods), leading to an atomic phase that also has a quadratic evolution with r and a radius of curvature given by

$$R_{\mathrm{atom}} = \frac{k_q W_{\mathrm{ir}}^2(z)}{4\alpha_q I_{\mathrm{ir}}} \quad (3)$$

where k_q is the qth harmonic wave vector. The spatial phase of the XUV beam in the emission plane is then also quadratic with r

$$\varphi_q(r,z) = \frac{k_q r^2}{2}\left(\frac{1}{R_{\mathrm{ir}}(z)} + \frac{1}{R_{\mathrm{atom}}(z)}\right) = \frac{k_q r^2}{2R(z)} \quad (4)$$

Under these assumptions, the XUV beam has all the characteristics (intensity profile and wavefront) of a Gaussian beam. The radii of curvature R_{ir} and R_{atom} can have comparable values when α_q is small (*19*). With α_q being positive, R_{atom} is positive, while R_{ir} can be either negative (for $z < 0$) or positive (for $z > 0$). The curvature of the XUV wavefront in the generating medium can therefore be controlled with the jet position, z_{jet}. For the long quantum path or in the cutoff where α_q is large (*19*), the impact of the atomic phase is often predominant and leads to XUV beams diverging in and after the generating medium. For the plateau harmonics emitted via the short quantum path that are considered in this paper, α_q is smaller and the XUV wavefront changes strongly with z_{jet}. As the spatial profile and wavefront are known in the generating plane, the spatial characteristics of these XUV Gaussian beams are known (*25*) for every longitudinal position, z (see Materials and Methods).

Simulated harmonic beam during propagation

To simulate our experiment, the IR fundamental beam centered at λ = 800 nm has a minimum beam waist W_{0_ir} = 83 μm located at z = 0. Harmonics are generated in neon with a peak intensity of 5.6×10^{14} W/cm^2 at focus. We take into account that α_q increases with the harmonic order (*22*, *26*–*29*) and consider a linear evolution from 5×10^{-14} cm^2/W for harmonic 29 to a constant value of 13×10^{-14} cm^2/W for harmonics 39 and above. The effective nonlinearity coefficient is q_{eff} = 4.7 (see Materials and Methods).

Figure 2 shows the XUV waist positions relative to the IR focus, z_{0_XUV} (Fig. 2A), and the waist size, W_{0_XUV} (Fig. 2B), for several harmonics as a function of the gas jet position. It shows that the XUV beam waists change strongly with the gas jet position and harmonic order. The harmonic foci are seldom located at the position of the IR focus and can be shifted by almost 30 cm from it. All harmonics exhibit a similar qualitative evolution, but each curve is shifted with respect to the jet position. The XUV waist positions differ significantly from one harmonic to the next as studied in (*7*), and we observe that this shift is strong for all jet positions. The shift between the harmonic waist positions is large not only as compared with the IR Rayleigh length ($Z_{\mathrm{r\_ir}}$ = 2.7 cm) but also as compared with the XUV beam's Rayleigh lengths. Figure 2B shows that the XUV beam waist, W_{0_XUV}, can change with z_{jet} between 3 and 60 μm, leading to Rayleigh lengths between 1 mm (W_{0_XUV} = 3 μm for H29) and 55 cm (W_{0_XUV} = 62 μm for

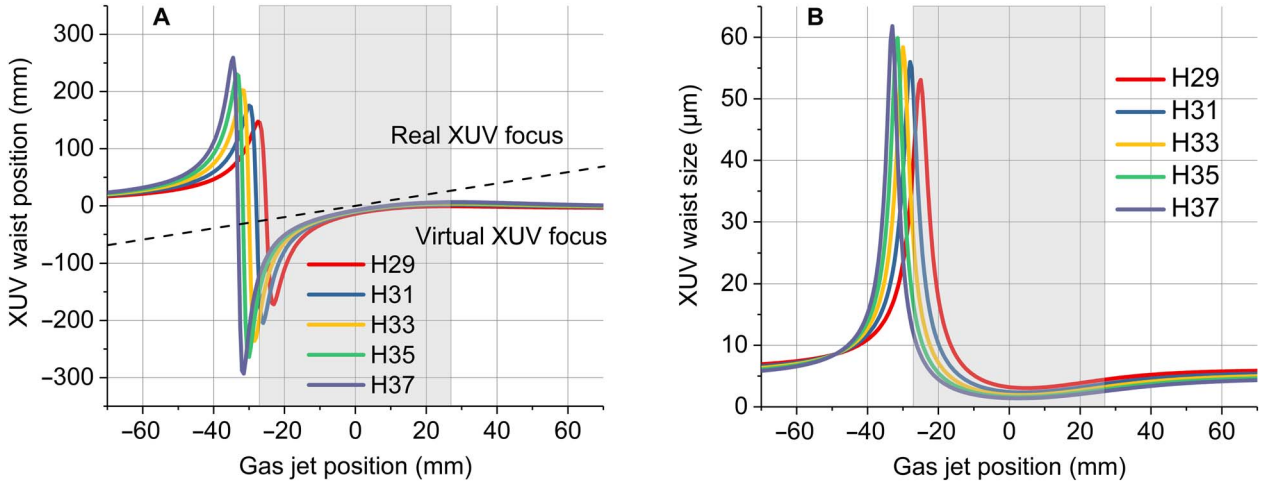

Fig. 2. Position and size of the XUV waists. (**A**) Calculated positions of the XUV beam waists, z_{0_XUV}, relative to the IR focus and (**B**) size of the harmonic beam waist, W_{0_XUV}. The IR focus is at $z = 0$, and negative positions imply a jet located before the IR focus. The shaded area represents the zone where the jet is within the IR beam Rayleigh range.

H37). This implies that when these harmonics are focused on a target, their foci positions can differ drastically. Therefore, the intensity and spectral width of the XUV radiation change locally near each harmonic focus (*7*, *9*, *14*). The harmonic dephasing is also modified by the Gouy phase shift occurring near focus, and the foci shift can strongly modify the XUV temporal profile.

In Fig. 2A, the dashed line indicates the gas jet position. Below this line, the XUV beam waists, located before the generating medium, are virtual. Above this line, the XUV waists located after the medium are real. Therefore, based on this model, we show that some harmonics can be emitted not only as diverging beams, as commonly assumed, but also as converging beams, leading to an XUV beam focused after the generating medium. To the best of our knowledge, optics-less focusing has never been studied experimentally before.

Now, we calculate the beam sizes in the far field and compare them with the experimental results. When the XUV beam waist is large, the beam divergence is small, leading to a small XUV beam size in the far field and vice versa. The XUV beam size calculated 2.9 m after the IR focus is plotted in Fig. 3, and its evolution qualitatively mimics our experimental observations. It shows a clear minimum for $z_{jet} = -25$ to -35 mm, followed by a maximum for $z_{jet} = 5$ to 10 mm with a maximum beam size that increases with the harmonic order. The minimum beam size is smaller than that in our measurement (0.5 mm versus 1.5 mm). It has a constant value for all harmonics and is shifted with the harmonic order as observed experimentally. If we consider that α_q changes with the IR peak intensity and therefore with z, the maxima and minima positions are shifted but the global trend is preserved (see the Supplementary Materials). These results show that the XUV beam characteristics are strongly affected by the generating conditions because they define the XUV wavefront in the generating medium and the XUV wavefront evolves dramatically with z_{jet}.

Overall, our measurements are in good qualitative agreement with the simulations and show how the spatial properties of the XUV beams can be finely controlled. These results demonstrate the intriguing possibility of focusing the harmonics after the generating medium without any optics.

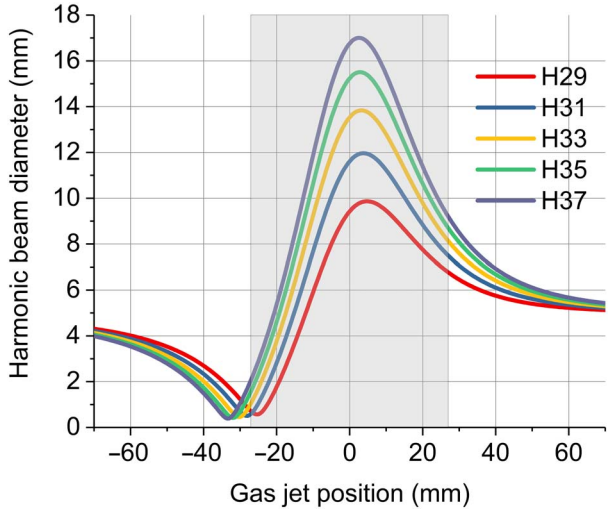

Fig. 3. Calculated diameters (FWHM) of the Gaussian XUV beams at a distance of 2.9 m after the IR focus position. The shaded area represents the zone where the jet is within the IR beam Rayleigh range.

XUV optics-less focusing

To further study the generation of harmonic beams focused via XUV wavefront control, we performed HHG with a spatially chirped fundamental beam (*30*, *31*) after transmitting the fundamental beam through a fused silica 2.5° wedge used near normal incidence. This reduces the intensity at focus and creates a spatial asymmetry in the spectral distribution of the fundamental beam (*32*, *33*). This asymmetry, acting as a probe inside the generation medium, spatially changes the central wavelength of the fundamental beam and of the emitted harmonics. The orientation of this spatial chirp was parallel to the entrance slit of the XUV spectrometer. The upper part of the IR beam was blue shifted, and the lower part was red shifted for all longitudinal z positions between $z = -40$ mm and $z = +40$ mm (see the Supplementary Materials), and the chirp was hardly measurable afterward. In the generating medium, harmonics emitted from the top of the IR beam are therefore blue shifted, and harmonics emitted from the

bottom of the IR beam are red shifted. In the far field, the spatiospectral distribution for each harmonic is recorded for several positions of the generating medium. The spatiospectral profiles for harmonic 29 are displayed in Fig. 4 for three jet positions. This beam exhibits a spatial chirp that changes with z_{jet}.

For a gas jet located 25 mm after the IR focus, the XUV beam has a spatial chirp with the same orientation as the IR spatial chirp in the generating medium (upper part blue shifted). This is expected if the XUV beam is emitted as a diverging beam since the upper part of the XUV beam in the emission plane is then also the upper part in the detection plane. On the contrary, we observe a chirp orientation inversion when the gas jet is located 70 mm before the IR focus. This implies that the upper part of the beam in the generating medium is the lower part of the beam in the far field. Therefore, the upper and lower parts of the beam overlap somewhere in between these two planes, confirming the optics-less focusing of the XUV beam.

The orientation of the spatial chirp in the far field is not defined for z_{jet} = −35 mm. This occurs when the XUV focus is located at the position of the gas jet (within less than the XUV Rayleigh length), since a perturbation spatially localized at the XUV focus is spatially delocalized in the far field. The XUV spatial chirps have the same orientation at z_{jet} = 0 mm and z_{jet} = +25 mm, implying that the XUV beam is already diverging in the jet at z_{jet} = 0. This shows directly that the XUV focus is not overlapped with the IR focus at z_{jet} = 0.

Our experiment also shows that the positions of the XUV foci depend on the harmonic order. The measured spatial chirps of harmonics 29 to 45 are shown in Fig. 5 for three jet positions.

Figure 5 shows that the orientation and magnitude of the far-field XUV spatial chirp change continuously with the harmonic order. For harmonic orders larger than 37, the spatial chirp has the same orientation as in the generating medium for all gas jet positions. These harmonics are always diverging in and after the generation medium, and the XUV beam waists are virtual. For z_{jet} = −50 mm, the spatial chirp is inverted for low-order harmonics (q < 35), meaning that these XUV beams are focused after the generating medium. The far-field spatial chirp of the XUV beam disappears when the XUV focus is located onto the jet (within the XUV Rayleigh range), and its orientation shows whether the waists are real or virtual. Observing an inversion of the spatial chirp with the harmonic order therefore confirms that for z_{jet} = −50 mm, the foci of harmonics 29 to 35 and 41 to 65 are located on the opposite sides of the generating medium and are separated by several XUV Rayleigh lengths. If these harmonic beams were refocused on a target, the XUV beams would not overlap significantly near their foci.

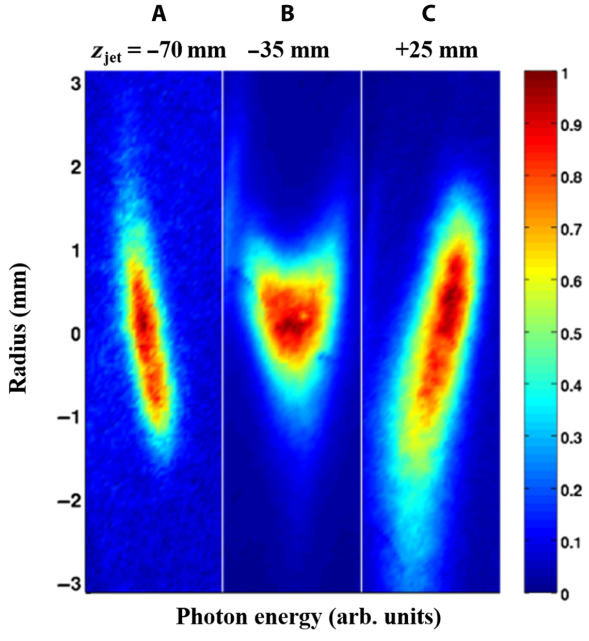

Fig. 4. Spatial chirp of harmonic 29. Far-field spatially resolved normalized spectra of the harmonic 29 generated in neon for three positions of the generating medium (**A**) z_{jet} = −70 mm, (**B**) z_{jet} = −35 mm, and (**C**) z_{jet} = +25 mm. HHG was performed with a fundamental beam that was spatially chirped in the generating medium. The tilt of the spatially resolved harmonic spectra is the signature of a spatial chirp in the XUV beam in the far field.

DISCUSSION

These results, obtained under standard HHG conditions, question how broadband XUV radiation should be used in attoscience experiments, since the harmonic foci relative shifts are large for all jet positions. This shift locally reduces the XUV bandwidth near each focus where a specific harmonic is enhanced. The first solution to maintain the XUV bandwidth is to image the HHG medium onto the target. In this image plane, each harmonic intensity is lower than that at the harmonic focus, but all the harmonics have similar spatial profiles, ensuring broadband irradiation. This limits the thickness of the target as the spatial overlap is reduced before and after the image plane. Another solution is to strongly reduce the XUV beam size in the far field with an iris before refocusing the beam on an experiment (*5*, *34*). The beam clipping enlarges the XUV Rayleigh lengths, and for strong clipping, the Rayleigh lengths can get larger than the relative foci shift. Both options reduce the useful XUV intensity, and it would be interesting to control the XUV beam characteristics to simultaneously obtain broadband irradiation and high XUV intensities. This can be done with controlled optics-less focusing as shown in the next paragraph. Alternatively, the XUV foci shift could be

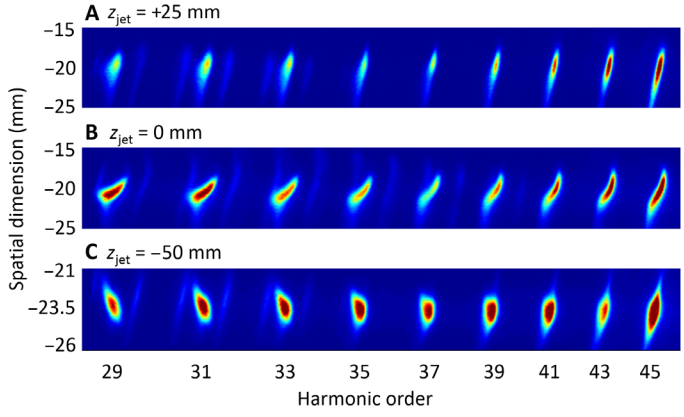

Fig. 5. Far-field XUV spatial chirp. Far-field spatially resolved high-order harmonic spectra obtained with a spatially chirped IR beam. The neon jet is located at various longitudinal positions (**A**) 25 mm after IR focus, (**B**) at IR focus, and (**C**) 50 mm before IR focus. The harmonic orders vary between 29 and 45 for the first order of diffraction of the XUV grating, and we observe the second orders of diffraction for harmonics 59 and higher. The tilt of the harmonic beams is the signature of a spatial chirp in the XUV beams in the far field. For the position z_{jet} = −50 mm, where the XUV beam is small, the spatial scale has been expanded.

used to perform spectral filtering of harmonic sources by locating a pinhole near the harmonic foci (*35*). The pinhole can transmit a specific harmonic group while reducing the transmission of other harmonics and of the fundamental beam. This provides an efficient spectral shaping with limited temporal stretching or even temporal compression when the attosecond pulses are strongly chirped before spectral selection (*36*).

Optics-less focusing has never been reported with standard HHG setup, but this effect is robust and likely universal when HHG occurs in a gas medium located before the laser focus. The control of the harmonic spatial characteristics via spatial coherence is demonstrated here with a beam having a Gaussian spatial profile. It can be extended by controlling the spatial profile and wavefront of the fundamental beam. Using a fundamental beam with a radially flat-top intensity profile (*37*) and a spherical wavefront would, for instance, make the optics-less focusing mostly independent on harmonic orders and laser peak intensity. Several harmonics could then be tightly refocused without any focusing optics over a large bandwidth compatible with broadband and intense attosecond irradiation. By considering the actual recorded value of XUV energy of 10 μJ per isolated attosecond pulse (*38*) and assuming a focusing on a 20-μm waist with a duration of 200 attoseconds, we estimate that XUV intensities larger than 10^{15} W/cm^2 can be achieved with optics-less focusing. Higher XUV intensities should even be accessible with higher-energy fundamental lasers (*39*). With precise wavefront control of an IR fundamental beam, this optics-less focusing can even be applied to focus harmonics generated in the soft x-ray domain that are harder to control spatially.

This study shows therefore that the spatial characteristics of XUV high-order harmonic beams generated in a thin medium can be controlled directly via a shaping of the XUV source wavefront and spatial distribution in the emission medium. We present a Gaussian model to infer the XUV beam spatial properties and show how the position of the XUV beam waists and the propagation characteristics of the XUV beams depend on both the harmonic order and the conditions of generation. By performing HHG in neon gas with a spatially filtered, wavefront-corrected, high-energy femtosecond laser, we demonstrate that the longitudinal gas medium displacement allows controlling the XUV beam properties and that plateau harmonic beams can be focused directly after the generating medium without resorting to any XUV focusing optics. The XUV beam waists can be virtual for some harmonics and real for others under the same generating conditions. The observed order-dependent foci shift implies that the harmonic foci are, in general, separated, and we show experimentally that their separation can be as large as several Rayleigh lengths of the XUV beams. We discuss how this relative foci shift is compatible with attosecond science and propose ways to use the optics-less focusing to perform XUV spectral filtering or achieve high XUV intensities.

MATERIALS AND METHODS

Experimental setup

We used a high-energy femtosecond fundamental IR (centered at λ_0 = 800 nm) pulse, and spatially filtered the laser beam before compression. Spatial filtering was performed under vacuum with a 250-μm pinhole after clipping the incoming beam with an iris and focusing it with a f = 1.3 m lens. The beam was afterward collimated with a spherical mirror located 1.5 m after the pinhole. The overall transmission of the spatial filtering was 50%, and output pulses with maximum energies of 50 mJ after compression could be used. When the spatial chirp was introduced, the pulse energy was limited to 2.5 mJ to limit nonlinear effects in the wedge.

The IR wavefront was corrected after compression under vacuum by a deformable mirror (High Power Active Mirror, Hipao, ISP Systems) that was specifically designed for high-energy ultrashort lasers. This active mirror is equipped with a thick glass membrane with multilayer dielectric coating that allows smooth correction and stable operation. The corrected IR wavefront, measured with an HASO (Imagine Optics), showed a residual error smaller than 8 nm rms (λ/100), and the Strehl ratio was larger than 0.95. Controlling the wavefront with such a high precision is crucial, since it ensures good XUV spatial coherence even when the harmonics are generated far from the IR focus position. Wavefront control was also used here to precompensate for the astigmatism induced by the spherical mirror used to focus the IR beam in the gas jet.

After corrections, we observed that the intensity profile of the fundamental beam was close to a Gaussian beam in the far field and near focus with a small asymmetry. The measured laser beam factor (M^2) was slightly different in the horizontal and vertical directions (see the Supplementary Materials), and we used a value of M^2 = 1.04 in the simulations. We measured a beam profile and size evolution with z that was close to a perfect Gaussian beam (see the Supplementary Materials), and we assumed in the simulations that the fundamental beam propagates (waist and wavefront dependence with z) as a Gaussian beam. The ability to control the IR wavefront with the deformable mirror has a large impact on the XUV beam, since it directly affects the XUV wavefront. It also ensures that the transverse evolution of the IR wavefront is regular even if far from the IR focus, while this is not always the case with a laser beam having a large M^2 factor that can exhibit complex phase evolution and additional spatial structures off-focus.

We used a 40-fs fundamental pulse with energy of ~2 to 5 mJ to generate high-order harmonics by focusing the input beam (W_x = 6.7 mm and W_y = 7.6 mm) truncated by a 20-mm-diameter iris with a f = 2 m spherical mirror to a focal spot size of $W_0 \approx$ 83 μm. The iris transmits most of the beam power and improves the beam symmetry near focus. HHG occurs at 10 Hz in a pulsed neon jet with a 250-μm nozzle diameter that could be moved by 7.5 cm before and after the IR focus. We analyzed the spatial profile of each harmonic in the far field with a flat field spectrometer. It is equipped with a 500-μm-wide entrance slit, a grazing incidence grating with 1200 grooves/mm (Hitachi aberration-corrected concave grating), and a 40-mm-diameter microchannel plate detector that was located 2.9 m after the IR focus position.

When HHG was performed with a spatially chirped beam, the fundamental beam was transmitted through a single fused silica 2.5° wedge used near normal incidence and located ~1.5 m before the focusing mirror. The wedge was located near a motorized folding mirror used to compensate for the average beam deviation introduced by the wedge and to maintain the same optical axis after the wedge.

Analytical method

Here, we neglected the propagation in the medium by considering an infinitely thin medium. Experimentally, this implies a loose focusing configuration and the use of conditions where the reshaping of the fundamental beam does not occur (*6*, *40*, *41*). For a medium that is only smaller than the IR beam confocal parameter, longitudinal phase matching can induce an additional amplitude prefactor (*23*) that can

slightly modify the XUV beam spatial profile in the generating medium. Note that optics-less focusing does not require perfect phase matching to occur and only requires that all angular components experience the same longitudinal phase-matching condition. In thick media, longitudinal phase matching/mismatch can also lead to the selection of a subset of XUV wave vectors that already exist with the thin medium considered here. It can however not lead to the creation of new XUV wave vectors, and thereby, the observations described here with a thin medium can also be obtained with extended media even if more complex calculations are required to simulate it. In general, our approach can be extended to more complex propagation situations, but this is beyond the scope of this paper, which focuses on the physics that allows controlling the spatial characteristics of coherent XUV beams obtained via HHG in gases.

In our model, we considered a single peak intensity even if the peak intensity changes with time in a real pulse. This approximation was done to mimic conditions under which a single attosecond pulse is emitted. Isolated attosecond pulse emission occurs at a specific time where the intensity is fixed. Averaging over several intensities could lead to a better agreement with experiments, and the value of the minimum would likely be bigger than that in these simulations after averaging over several intensities. It could also lead to a more limited apparent beam evolution and can reduce the apparent foci shift. However, we stress that when a single attosecond pulse is generated, the emission time corresponds to a single peak intensity; therefore, our simulations, providing the beam shape at a specific time, are relevant to highlight the underlying physics.

The atomic phase of the model dipole is

$$\varphi_{\text{atom}}(r) = -\alpha_q I(z_{\text{jet}})\exp(-2r^2/W_{\text{ir}}(z_{\text{jet}})^2) \quad (5)$$

It is simplified by performing a Taylor expansion of the Gaussian IR intensity profile near the laser axis that leads to a quadratic phase

$$\varphi_{\text{atom}}(r) = k_q r^2/2R_{\text{atom}} \quad (6)$$

with

$$R_{\text{atom}} = \pi {W_{\text{ir}}}^4/2\alpha_q I_0 {W_{0\_\text{ir}}}^2\lambda_q \quad (7)$$

where λ_q is the harmonic wavelength, W_{0_ir} is the IR beam waist size at focus, W_{ir} is the IR beam size at the jet position, and I_0 is the peak intensity at focus. Since the IR wavefront is also quadratic with radius of curvature R_{ir}, the emitted XUV wavefront is spherical with a radius of curvature R given by $1/R = 1/R_{\text{ir}} + 1/R_{\text{atom}}$.

The XUV intensity profile is Gaussian in the generating medium, and its size is linked to the IR beam size via the effective order of nonlinearity q_{eff} (Eq. 2). With a Gaussian spatial profile and a spherical wavefront, the XUV beams have all the characteristics of regular Gaussian beams, and from standard Gaussian propagation law (*25*), we obtained analytical formulas for both the XUV focus position, z_{0_XUV}, as compared to the IR focus and the harmonic waist size, W_{0_XUV}

$$z_{0\_\text{XUV}} = z_{\text{jet}} - R/(1 + R^2{\lambda_q}^2{q_{\text{eff}}}^2/(\pi^2{W_{\text{ir}}}^4)) \quad (8)$$

$$W_{0\_\text{XUV}} = \left[\left(R^2{\lambda_q}^2 q_{\text{eff}}/\left(\pi^2{W_{\text{ir}}}^2\right)\right)/\left(1 + R^2{\lambda_q}^2{q_{\text{eff}}}^2/\left(\pi^2{W_{\text{ir}}}^4\right)\right)\right]^{1/2} \quad (9)$$

The displacement of the XUV waist position, z_{0_XUV}, depends on the XUV wavefront radius of curvature, R, in the generating medium. When z_{jet} is neglected, this displacement is maximum for

$$R^2{\lambda_q}^2{q_{\text{eff}}}^2/(\pi^2{W_{\text{ir}}}^4) = 1 \quad (10)$$

which gives a radius of curvature

$$R = -\pi {W_{\text{ir}}}^2/(\lambda_q q_{\text{eff}}) \quad (11)$$

The maximum shift of the XUV waist position is therefore

$$z_{0\_\text{XUV}} = -R/2 = (\pi {W_{\text{ir}}}^2)/(2\lambda_q q_{\text{eff}}) \quad (12)$$

that can be expressed as

$$z_{0\_\text{XUV}} = 1/2\, z_{r\_\text{ir}}(W_{\text{ir}}/W_{0\_\text{ir}})^2 q/q_{\text{eff}} \quad (13)$$

This analytical expression given by Eq. 13 shows that the XUV beam can be focused far from the IR focus, provided that q_{eff} is smaller than the harmonic order (always correct in the tunneling regime) and provided that the harmonic generation takes place off focus where W_{ir} is significantly larger than W_{0_ir}.

The size of the XUV waist, W_{0_XUV}, can also be estimated at this maximum shift by combining Eqs. 9 and 11, which leads to

$$W_{0\_\text{XUV}} = \frac{1}{\sqrt{2}}\frac{W_{\text{ir}}}{\sqrt{q_{\text{eff}}}} \quad (14)$$

This last formula shows that when the focus is at the maximum shift, the XUV beam waist is independent of the XUV wavelength and is equal to the size of the XUV beam in the gas jet divided by $\sqrt{2}$. It also implies that the maximum foci shift is the XUV Rayleigh length that can be arbitrarily large for extended XUV sources. This estimate gives the waist located at the maximum distance of the generating medium, and these waists are large at that position. A smaller XUV waist can be obtained closer to the generating medium (Fig. 1B), and controlling the generating medium position is a way to control the XUV waist size and location between this maximum shift and a minimum waist size obtained near the IR focus.

Equations 8 and 9 also show that the largest XUV waists are obtained when the XUV foci overlap with the generating medium (obtained around $z = -30$ mm in Fig. 3). In return, this shows that the maximum waist size is similar for all harmonics, provided that q_{eff} is approximately constant. This implies that the minimum beam size in the far field must be nearly identical for all harmonics as observed experimentally.

We note that the harmonic foci shift depends on the fundamental wavelength that strongly affects not only q/q_{eff} but also the value of α_q, since its asymptotic value (α value in the cutoff that represents a

scaling factor in the optics-less focusing) is proportional to the third power of the laser frequency (*23*, *29*). Mid-IR and far-IR fundamental lasers are now used to obtain broadband harmonic plateaus, and we anticipate that the cutoff harmonic will be focused very far from the lowest plateau harmonics and that the harmonic foci shift should be very pronounced with these lasers. For a specific fundamental wavelength, the relative foci shift between consecutive harmonics depends on the evolution of the α_q parameter between each harmonic. This parameter is close to zero near I_p for short-trajectory harmonics and close to an asymptotic value mostly defined by the fundamental wavelength near the cutoff. Therefore, for a given fundamental wavelength, the α_q change between each harmonic is more pronounced for a narrower plateau. Thus, the foci shift, shown here when neon atoms are used for HHG, should also be observable with other generating gases such as Xe, Kr, or Ar (*7*), which leads to narrower plateaus but faster evolution of the α_q term between adjacent harmonics.

SUPPLEMENTARY MATERIALS

Supplementary material for this article is available at http://advances.sciencemag.org/cgi/content/full/5/4/eaau7175/DC1

Section S1. Experimental setup
Section S2. Characterization of the IR spatial chirp near focus
Section S3. Evolution of the HHG efficiency with the jet longitudinal position
Section S4. Evolution of the beam size for higher-order harmonics
Section S5. Impact of q_{eff} and α on the numerical results
Section S6. Impact of the longitudinal evolution of α
Section S7. Normalized focus shift
Section S8. Simulations with non-Gaussian XUV beams
Fig. S1. Spatial profile of the fundamental beam.
Fig. S2. Experimental setup.
Fig. S3. Characterization of the spatial chirp near the focus of the IR beam.
Fig. S4. Integrated XUV emission.
Fig. S5. Diameter of the XUV beam in the far field.
Fig. S6. Parametric evolution of the XUV beam size.
Fig. S7. Influence of the α parameter.
Fig. S8. Beam size evolution for several peak intensities.
Fig. S9. Normalized focus shift.
Fig. S10. Non-Gaussian XUV beam size evolution.

REFERENCES AND NOTES

1. G. Sansone, L. Poletto, M. Nisoli, High-energy attosecond light sources. *Nat. Photonics* **5**, 655–663 (2011).
2. C. M. Heyl, H. Coudert-Alteirac, M. Miranda, M. Louisy, K. Kovacs, V. Tosa, E. Balogh, K. Varjú, A. L'Huillier, A. Couairon, C. L. Arnold, Scale-invariant nonlinear optics in gases. *Optica* **3**, 75–81 (2016).
3. T. Popmintchev, M.-C. Chen, P. Arpin, M. M. Murnane, H. C. Kapteyn, The attosecond nonlinear optics of bright coherent x-ray generation. *Nat. Photonics* **4**, 822–832 (2010).
4. M. Nisoli, E. Priori, G. Sansone, S. Stagira, G. Cerullo, S. De Silvestri, C. Altucci, R. Bruzzese, C. de Lisio, P. Villoresi, L. Poletto, M. Pascolini, G. Tondello, High-brightness high-order harmonic generation by truncated bessel beams in the sub-10-fs regime. *Phys. Rev. Lett.* **88**, 033902 (2002).
5. M. B. Gaarde, K. J. Schafer, Generating single attosecond pulses via spatial filtering. *Opt. Lett.* **31**, 3188–3190 (2006).
6. M. B. Gaarde, J. L. Tate, K. J. Schafer, Macroscopic aspects of attosecond pulse generation. *J. Phys. B At. Mol. Opt. Phys.* **41**, 132001 (2008).
7. E. Frumker, G. G. Paulus, H. Niikura, A. Naumov, D. M. Villeneuve, P. B. Corkum, Order-dependent structure of high harmonic wavefronts. *Opt. Express* **20**, 13870–13877 (2012).
8. A. Dubrouil, O. Hort, F. Catoire, D. Descamps, S. Petit, E. Mével, V. V. Strelkov, E. Constant, Spatio–spectral structures in high-order harmonic beams generated with Terawatt 10-fs pulses. *Nat. Commun.* **5**, 4637 (2014).
9. D. T. Lloyd, K. O'Keefe, P. N. Anderson, S. M. Hooker, Gaussian-Schell analysis of the transverse spatial properties of high-harmonic beams. *Sci. Rep.* **6**, 30504 (2016).
10. Z. Li, G. Brown, D. H. Ko, F. Kong, L. Arissian, P. B. Corkum, Perturbative high harmonic wave front control. *Phys. Rev. Lett.* **118**, 033905 (2017).
11. M. Sivis, M. Taucer, G. Vampa, K. Johnston, A. Staudte, A. Y. Naumov, D. M. Villeneuve, C. Ropers, P. B. Corkum, Tailored semiconductors for high-harmonic optoelectronics. *Science* **357**, 303–306 (2017).
12. N. Dudovich, J. L. Tate, Y. Mairesse, D. M. Villeneuve, P. B. Corkum, M. B. Gaarde, Subcycle spatial mapping of recollision dynamics. *Phys. Rev. A* **80**, 011806(R) (2009).
13. O. Kfir, M. Kozlov, A. Fleischer, O. Cohen, Attosecond pulses with sophisticated spatio-spectral waveforms: Spatio-spectral Airy and auto-focusing beams. *Opt. Express* **19**, 21730–21738 (2011).
14. V. T. Platonenko, V. V. Strelkov, Single attosecond soft-x-ray pulse generated with a limited laser beam. *J. Opt. Soc. Am. B* **16**, 435–440 (1999).
15. P. Tzallas, D. Charalambidis, N. A. Papadogiannis, K. Witte, G. D. Tsakiris, Direct observation of attosecond light bunching. *Nature* **426**, 267–271 (2003).
16. T. Sekikawa, A. Kosuge, T. Kanai, S. Watanabe, Nonlinear optics in the extreme ultraviolet. *Nature* **432**, 605–608 (2004).
17. T. Okino, Y. Furukawa, T. Shimizu, Y. Nabekawa, K. Yamanouchi, K. Midorikawa, Nonlinear Fourier transformation spectroscopy of small molecules with intense attosecond pulse train. *J. Phys. B At. Mol. Opt. Phys.* **47**, 124007 (2014).
18. B. Manschwetus, L. Rading, F. Campi, S. Maclot, H. Coudert-Alteirac, J. Lahl, H. Wikmark, P. Rudawski, C. M. Heyl, B. Farkas, T. Mohamed, A. L'Huillier, P. Johnsson, Two-photon double ionization of neon using an intense attosecond pulse train. *Phys. Rev. A* **93**, 061402(R) (2016).
19. M. Lewenstein, P. Salières, A. L'Huillier, Phase of the atomic polarization in high-order harmonic generation. *Phys. Rev. A* **52**, 4747–4754 (1995).
20. M. B. Gaarde, F. Salin, E. Constant, P. Balcou, K. J. Schafer, K. C. Kulander, A. L'Huillier, Spatiotemporal separation of high harmonic radiation into two quantum path components. *Phys. Rev. A* **59**, 1367–1373 (1999).
21. E. Constant, D. Garzella, P. Breger, E. Mével, C. Dorrer, C. Le Blanc, F. Salin, P. Agostini, Optimizing high harmonic generation in absorbing gases: Model and experiment. *Phys. Rev. Lett.* **82**, 1668–1671 (1999).
22. S. Carlström, J. Preclíková, E. Lorek, E. W. Larsen, C. M. Heyl, D. Paleček, D. Zigmantas, K. J. Schafer, M. B. Gaarde, J. Mauritsson, Spatially and spectrally resolved quantum path interference with chirped driving pulses. *New J. Phys.* **18**, 123032 (2016).
23. F. Catoire, A. Ferré, O. Hort, A. Dubrouil, L. Quintard, D. Descamps, S. Petit, F. Burgy, E. Mével, Y. Mairesse, E. Constant, Complex structure of spatially resolved high-order-harmonic spectra. *Phys. Rev. A* **94**, 063401 (2016).
24. L. Rego, J. S. Román, A. Picón, L. Plaja, C. Hernández-García, Nonperturbative twist in the generation of extreme-ultraviolet vortex beams. *Phys. Rev. Lett.* **117**, 163202 (2016).
25. H. Kogelnik, T. Li, Laser beams and resonators. *Appl. Opt.* **5**, 1550–1567 (1966).
26. M. B. Gaarde, K. J. Schafer, Quantum path distributions for high-order harmonics in rare gas atoms. *Phys. Rev. A* **65**, 031406(R) (2002).
27. C. Corsi, A. Pirri, E. Sali, A. Tortora, M. Bellini, Direct interferometric measurement of the atomic dipole phase in high-order harmonic generation. *Phys. Rev. Lett.* **97**, 023901 (2006).
28. L. He, P. Lan, Q. Zhang, C. Zhai, F. Wang, W. Shi, P. Lu, Spectrally resolved spatiotemporal features of quantum paths in high-order-harmonic generation. *Phys. Rev. A* **92**, 043403 (2015).
29. M. A. Khokhlova, V. V. Strelkov, Phase properties of the cutoff high-order harmonics. *Phys. Rev. A* **93**, 043416 (2016).
30. H. Vincenti, F. Quéré, Attosecond lighthouses: How to use spatiotemporally coupled light fields to generate isolated attosecond pulses. *Phys. Rev. Lett.* **108**, 113904 (2012).
31. F. Quéré, H. Vincenti, A. Borot, S. Monchocé, T. J. Hammond, K. T. Kim, J. A. Wheeler, C. Zhang, T. Ruchon, T. Auguste, J. F. Hergott, D. M. Villeneuve, P. B. Corkum, R. Lopez-Martens, Applications of ultrafast wavefront rotation in highly nonlinear optics. *J. Phys. B At. Mol. Opt. Phys.* **47**, 124004 (2014).
32. Z. Guang, M. Rhodes, R. Trebino, Measurement of the ultrafast lighthouse effect using a complete spatiotemporal pulse-characterization technique. *J. Opt. Soc. Am. B* **33**, 1955–1962 (2016).
33. C. Herńandez-García, A. Jaron-Becker, D. D. Hickstein, A. Becker, C. G. Durfee, High-order-harmonic generation driven by pulses with angular spatial chirp. *Phys. Rev. A* **93**, 023825 (2016).
34. M. Hentschel, R. Kienberger, C. Spielmann, G. A. Reider, N. Milosevic, T. Brabec, P. Corkum, U. Heinzmann, M. Drescher, F. Krausz, Attosecond metrology. *Nature* **414**, 509–513 (2001).
35. V. T. Platonenko, V. V. Strelkov, Generation of a single attosecond x-ray pulse. *Quantum Electron.* **28**, 749–753 (1998).
36. Y. Mairesse, A. de Bohan, L. J. Frasinski, H. Merdji, L. C. Dinu, P. Monchicourt, P. Breger, M. Kovačev, R. Taïeb, B. Carré, H. G. Muller, P. Agostini, P. Salières, Attosecond synchronization of high-harmonic soft x-rays. *Science* **302**, 1540–1543 (2003).
37. A. Dubrouil, Y. Mairesse, B. Fabre, D. Descamps, S. Petit, E. Mével, E. Constant, Controlling high harmonics generation by spatial shaping of high energy femtosecond beam. *Opt. Lett.* **36**, 2486–2488 (2011).

38. E. J. Takahashi, P. Lan, O. D. Mücke, Y. Nabekawa, K. Midorikawa, Attosecond nonlinear optics using gigawatt-scale isolated attosecond pulses. *Nat. Commun.* **4**, 2691 (2013).
39. S. Kühn, M. Dumergue, S. Kahaly, S. Mondal, M. Füle, T. Csizmadia, B. Farkas, B. Major, Z. Várallyay, E. Cormier, M. Kalashnikov, F. Calegari, M. Devetta, F. Frassetto, E. Månsson, L. Poletto, S. Stagira, C. Vozzi, M. Nisoli, P. Rudawski, S. Maclot, F. Campi, H. Wikmark, C. L. Arnold, C. M. Heyl, P. Johnsson, A. L'Huillier, R. Lopez-Martens, S. Haessler, M. Bocoum, F. Boehle, A. Vernier, G. Iaquaniello, E. Skantzakis, N. Papadakis, C. Kalpouzos, P. Tzallas, F. Lépine, D. Charalambidis, K. Varjú, K. Osvay, G. Sansone, The ELI-ALPS facility: The next generation of attosecond sources. *J. Phys. B At. Mol. Opt. Phys.* **50**, 132002 (2017).
40. W. Holgado, B. Alonso, J. San Román, I. J. Sola, Temporal and spectral structure of the infrared pulse during the high order harmonic generation. *Opt. Express* **22**, 10191–10201 (2014).
41. V. Tosa, E. Takahashi, Y. Nabekawa, K. Midorikawa, Generation of high-order harmonics in a self-guided beam. *Phys. Rev. A* **67**, 063817 (2003).

Acknowledgments: We acknowledge the stimulating discussions with F. Lépine, V. Loriot, K. Veyrinas, and C. Valentin. **Funding:** We acknowledge funding from the region Aquitaine (Caracatto 2013–1603008 and Hipao programs), the CNRS (Pics no. PICS06038), the ANR (ANR-09-BLAN-0031-02 Attowave and ANR-16-CE30-0012 Circé), the Université de Bordeaux for providing access to the Mésocentre de Calcul Intensif Aquitain (MCIA), and RFBR (grant no. 19-02-00739). Preliminary theoretical studies showing the existence of optics-less focusing were supported by the RSF (grant no. 16-12-10279). **Author contributions:** L.Q., E.M., and E.C. performed the experiments. E.C. and E.M. conceived the experiments and, together with O.H., A.D., D.D., F.B., and C.P., developed the apparatus. F.C., J.V., and V.S. developed the simulations. L.Q. and E.C. performed the data analysis. E.C. carried out the first drafting of the manuscript. All authors contributed to the final version of the manuscript. **Competing interests:** The authors declare that they have no competing interests. **Data and materials availability:** All data needed to evaluate the conclusions in the paper are present in the paper and/or the Supplementary Materials. Additional data related to this paper may be requested from the authors.

Submitted 9 July 2018
Accepted 12 February 2019
Published 5 April 2019
10.1126/sciadv.aau7175

Citation: L. Quintard, V. Strelkov, J. Vabek, O. Hort, A. Dubrouil, D. Descamps, F. Burgy, C. Péjot, E. Mével, F. Catoire, E. Constant, Optics-less focusing of XUV high-order harmonics. *Sci. Adv.* **5**, eaau7175 (2019).

Optics-less focusing of XUV high-order harmonics

L. Quintard, V. Strelkov, J. Vabek, O. Hort, A. Dubrouil, D. Descamps, F. Burgy, C. Péjot, E. Mével, F. Catoire and E. Constant

Sci Adv **5** (4), eaau7175.
DOI: 10.1126/sciadv.aau7175